On the Overdrawing of Melt-Spun Isotactic Polypropylene Tapes

Tilo Schimanski,[1] Joachim Loos,[1,2] Ton Peijs,[1,2,3] Ben Alcock,[1,2,3] Piet J. Lemstra[1,2]

[1]*Laboratory of Polymer Technology, Department of Chemical Engineering and Chemistry, Eindhoven University of Technology, P.O. Box 513, 5600 MB Eindhoven, The Netherlands*
[2]*Dutch Polymer Institute, Eindhoven University of Technology, P.O. Box 513, 5600 MB Eindhoven, The Netherlands*
[3]*Department of Materials, Queen Mary University of London, Mile End Road, London E1 4NS, United Kingdom*

Received 19 May 2006; accepted 29 June 2006
DOI 10.1002/app.25128
Published online in Wiley InterScience (www.interscience.wiley.com).

ABSTRACT: The morphology and mechanical properties of melt-spun and post-drawn isotactic polypropylene (iPP) tapes have been studied in order to examine their dependence on the post-draw ratio applied. Special attention is focused on the characterization of the so-called overdrawing behavior of the tapes; at a certain draw ratio, a change of the optical appearance of the tape from transparent to opaque is observed. Overdrawing is accompanied with changes in the mechanical properties, surface, and morphology of the tapes. For post-draw ratios without overdrawing, and for highly overdrawn tapes, the variation in the mechanical properties measured is very small, but for slightly overdrawn tapes, a large scattering of mechanical properties has been measured. In the latter case, this behavior is related to the start of internal delamination of the tapes during post drawing. It is shown that strongly overdrawn tapes have excellent mechanical properties, in particular, high specific stiffness and strength. © 2006 Wiley Periodicals, Inc. J Appl Polym Sci 103: 2920–2931, 2007

Key words: isotactic polypropylene (iPP); melt spinning; solid-state drawing; morphology; overdrawing; mechanical properties

INTRODUCTION

Fundamental studies on the melt spinning of isotactic polypropylene date back to the 1960s, immediately following the emergence of the commercial significance of polymers.[1–3] The influence of spinning conditions, such as extrusion temperature, take-up velocity, or spin-line stress, as well as material characteristics (mainly, the molecular mass and the molecular mass distribution), has been reported extensively in the literature.[4–9] Fibres/tapes produced by high-speed melt spinning offer mechanical properties which are adequate for a number of commodity applications (e.g., textiles and carpets). However, obtaining fibers/tapes with mechanical properties suitable for advanced engineering applications requires extending and orienting the molecules in an additional solid-state post-drawing operation.[9–14] In many studies the dependence of mechanical properties on the applied draw ratio is described for solid-state drawn fibrous structures. It is commonly concluded that stiffness and strength increase with increasing draw ratio, while elongation at break decreases.[14–15]

In the present study, special attention is directed to the so-called phenomenon of 'overdrawing'. At a certain draw ratio, a change of the fiber/tape optical appearance is observed. An opaque layer starts to develop in the centre of the formerly transparent fiber/tape. This layer widens over the complete fiber diameter or tape width with further increasing draw ratio. The structure and morphology of overdrawn polypropylene fibers was studied intensively by Bassett et al.[16] They attributed the development of opaqueness in overdrawn fibers to the appearance of density fluctuations within the sample. However, they have not investigated the influence of features related to overdrawing on the mechanical properties of fibers. It is the main objective of our study to link mechanical properties and morphology of melt-spun and overdrawn iPP tapes with their mechanical behavior; and to explore the drawbacks and/or benefits of overdrawing for the manufacturing of stiff and strong iPP fibers or tapes for engineering applications. For this reason, structure and morphology of tapes post-drawn to ratios (λ_{PDR}) varying from $\lambda_{PDR} = 2$ to $\lambda_{PDR} = 15$ were characterized by density measurements, low-voltage scanning electron microscopy (LVSEM), confocal laser scanning microscopy (CLSM), and wide-angle X-ray scattering (WAXS). The corresponding mechanical properties were measured at room temperature using a tensile tester.

EXPERIMENTAL

The tapes were produced from an isotactic polypropylene homopolymer, X-7284, kindly supplied by DSM, The Netherlands. The material possesses a weight average molar mass of $M_w = 280$ kg mol^{-1}, a

Correspondence to: J. Loos (j.loos@tue.nl).

Journal of Applied Polymer Science, Vol. 103, 2920–2931 (2007)

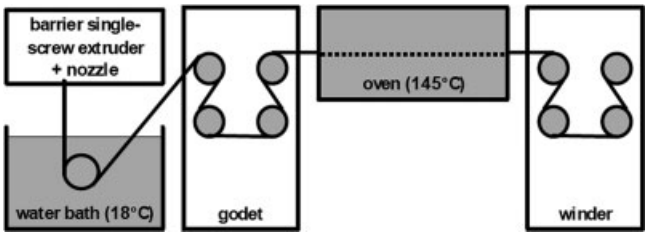

Figure 1 Schematic drawing of the melt spinning and solid-state drawing line.

polydispersity of $M_w/M_n = 5.8$ and a melt-flow index (MFI) of 13. The tapes were prepared on a research and development (R&D) tape drawing line at Lankhorst Indutech B.V., The Netherlands. This drawing line consists of an extruder, a nozzle, a water bath (18°C), a godet, an oven, and a winder. The line approximates an industrial scale production, allowing the transfer of data between the R&D line and a commercial production line. A schematic drawing of the R&D line is shown in Figure 1. The extruder is a special barrier single-screw extruder with a screw diameter of 30 mm. The output of the extruder is controlled by the screw rotation frequency and was kept constant. The post-draw ratio (λ_{PDR}) within the oven is determined by the ratio of the winder speed to the godet speed. For the studied samples, the godet speed was kept constant at 8 m min^{-1}. Different post-draw ratios were obtained by adjusting the velocity of the winder correspondingly. All other processing parameters were kept constant. In the (hot-air) oven with a length of approximately 3 m, the tape was post-drawn at a temperature of 145°C. It has to be emphasised that the temperature reported is not the temperature of the tape but the adjusted temperature of the oven. Unfortunately, both the thermal conditions inside the oven (e.g., velocity of the hot air) as well as the strain rate of the tape as a function of the position in the oven are unknown. Therefore, it is not possible to calculate the tape temperature accurately. However, a first-order approximation based on heat convection shows that the tape temperature approaches the oven temperature with increasing residence time in the oven. It is assumed that for the drawing conditions chosen the tape temperature is close to the oven temperature.

The mechanical properties of the tapes were measured at room temperature using a tensile tester equipped with an extensometer, force-reducing clamps, and a load-cell of 500 N. The tensile tests were carried out with tapes of initial gauge length of 150 mm and at a cross-head speed of 150 mm min^{-1}. Force-elongation curves were recorded on a central section of the tapes with a length of 50 mm, as shown in Figure 2. A preload of about 0.5 N was applied on the samples prior to testing. A set of 10 tensile tests was performed on each tape. In order to relate the tensile force to the cross-section area, the thickness and width of the tapes were measured. The thickness was determined using a TWIN-CHECK layer thickness instrument via a magnetic-inductive method. The instrument has a relative accuracy of 1%. The width was measured with a magnifying glass equipped with a scale-bar. For both dimensions, the average of 20 independent measurements, spread over a tape length of 20 m, was taken as the representative value. The obtained average values were also compared with the corresponding theoretical values calculated from a purely uniaxial deformation for the following assumptions:

i. constant volume $\lambda_l\ \lambda_t\ \lambda_w = 1$, where subscripts l, t and w represent length, thickness and width of the tape, respectively;
ii. isotropic drawing behavior in the lateral dimensions $\lambda_t = \lambda_w$.

The theoretical thickness (t) for a certain draw ratio λ results from

$$t = \frac{t_0}{\sqrt{\lambda}} \tag{1}$$

where t_0 represents the initial thickness of the tape before drawing.

The same equation can be used to calculate the theoretical width w by replacing t and t_0 by w and w_0, respectively. In order to generate theoretical curves, which are independent of the dimensions of the as-extruded precursor tape, the values for t and w were

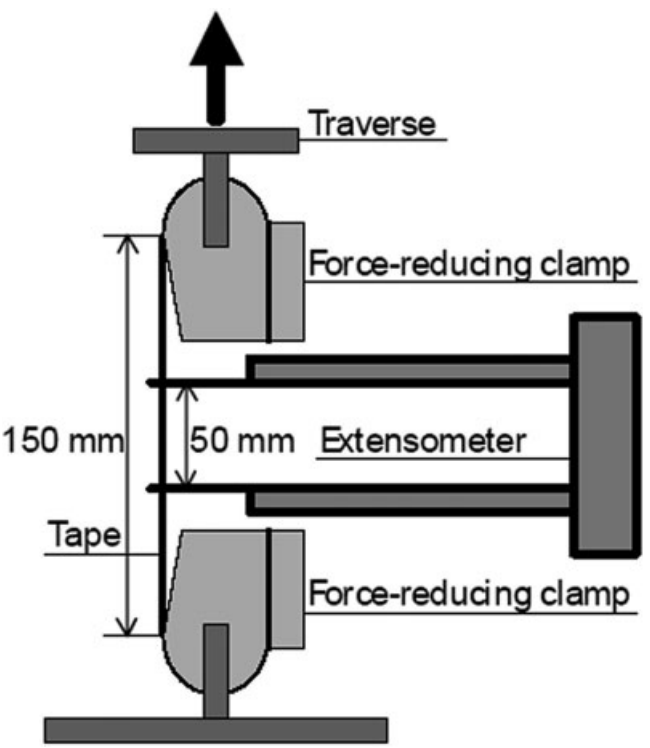

Figure 2 Schematic drawing of the tensile test device.

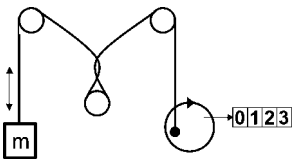

Figure 3 Schematic drawing of the abrasion tester.

normalized by dividing by t_0 and w_0, respectively. The authors are aware of the slight inaccuracy in the theoretical thickness/width obtained by the assumption of constant volume. It is more precise to assume conservation of mass, which takes into account changes in density while post-drawing. For constant mass, eq. (1) changes to:

$$t = \frac{t_0}{\sqrt{\lambda \frac{\rho}{\rho_0}}} \tag{2}$$

where ρ and ρ_0 are the densities of the drawn tape and the as-extruded tape, respectively. However, density measurements on a series of post-drawn tapes with $\lambda_{PDR} = 2$ to $\lambda_{PDR} = 15$ revealed a variation in density smaller than 2% compared to the density of the as-extruded tape. Therefore, corrections for the theoretical thickness obtained by the assumption of constant mass are very small and have been neglected.

The density of the tapes was measured at room temperature using a density-gradient column. The column had a density gradient from 880 kg m^{-3} to 930 kg m^{-3} and was prepared using distilled water and isopropyl alcohol according to the method described by Tung and Taylor.[17] The samples were allowed to seek their equilibrium position in the column for approximately 6 h. The shrinkage behavior of the tapes was investigated by immersion in a warmed oil bath for 120 sec at 100°C. Subsequently, the shrinkage was determined as a percentage of the original sample length of 300 mm.

Abrasion resistance of the tapes with $\lambda_{PDR} = 7$ to $\lambda_{PDR} = 15$ was measured by using a custom-made laboratory-scale abrasion tester. A schematic drawing of this instrument is shown in Figure 3. One end of the tape is fixed to a rotating disk, while the other end is connected to a load. The tape is looped over an additional wheel in such a way that disc rotation causes abrasion between two crossing areas of the tape. In order to ensure constant tension, the load is adjusted correspondingly to the cross-section area of the tape. A counter records the number of disk rotations until the failure of the tape.

Scanning electron microscopy (SEM) examinations were performed on the tapes using a Philips XL-30 ESEM-FEG environmental scanning electron microscope. Investigations were carried out under low-voltage (LVSEM) conditions using an acceleration voltage of 1 to 5 kV in order to prevent charging. In this mode, no conductive surface coating is required. A secondary electron (SE) detector was used to monitor the morphology of the samples. Additional LVSEM investigations were performed on a tape with $\lambda_{PDR} = 15$, which was etched with a permanganic reagent (0.7% $KMnO_4$ in 10 : 4 : 1 H_2SO_4 : H_3PO_4 : H_2O) for 2 h at room temperature and then washed according to standard procedures.[18]

The morphology of the surface and the bulk of the tape with $\lambda_{PDR} = 15$ was also investigated with a confocal laser scanning microscope (Zeiss LSM 510) in reflection mode. This technique allows 'optical slicing' of the sample by focusing the laser at different depths in the sample. Afterwards, a software program can convert the recorded images into an image of the cross-section of the sample. Wide-angle X-ray diffraction (WAXD) patterns were recorded on a transmission pinhole camera with an exposure time of 3 h. A Philips PW-1120 X-ray generator working at 40 kV and 30 mA produced the X-rays. The Cu-K_α radiation had an average wavelength of 1.542Å, while the Cu-K_β radiation was eliminated by a Ni-filter. The 2D X-ray patterns were transformed into 1D patterns by performing integration along the azimuthal angle. Afterwards, the integrated pattern was used to determine the position of the peak maximum of each reflection. At this particular angle, the azimuthal intensity distribution was measured in the 2D pattern. The full-width at half-maximum (FWHM) of the obtained intensity distribution pattern was calculated as a normalized measure for the arc length of the reflection.

RESULTS

Morphology of overdrawn tapes

Figure 4 shows the optical appearance of the tapes. They are gradually arranged with increasing post-draw ratio from the left to the right, starting with the as-extruded tape (as extruded, $\lambda_{PDR} = 2, \ldots, \lambda_{PDR} = 15$). The width of the tapes decreases with increasing post-draw ratio, and for draw ratios above 10 the appearance of the tapes change from transparent to

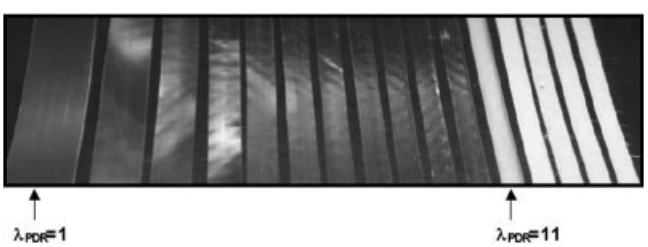

Figure 4 Optical appearance of the post-drawn tapes starting on the left side with the as-extruded tape (as-extruded ($\lambda_{PDR} = 1$), $\lambda_{PDR} = 2, \ldots, \lambda_{PDR} = 10$, $\lambda_{PDR} = 10.5$, $\lambda_{PDR} = 11, \ldots, \lambda_{PDR} = 15$). There is a clear transition from transparent to opaque tape structure at $\lambda_{PDR} \geq 11$.

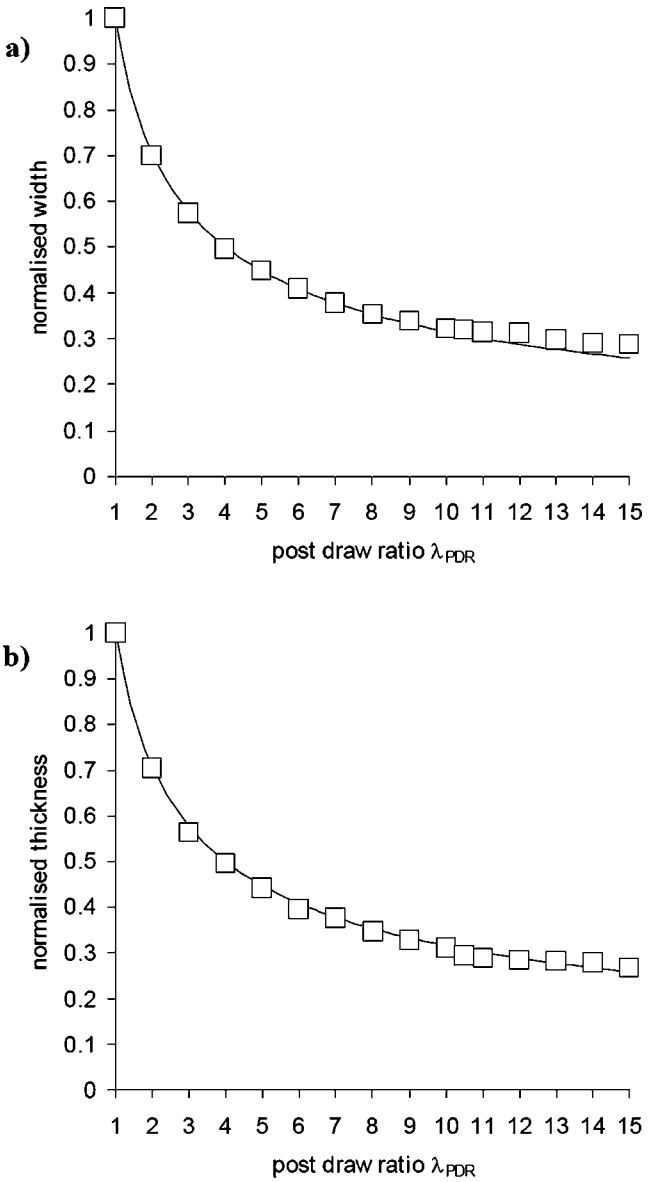

Figure 5 Normalized (a) width and (b) thickness as a function of the post-draw ratio, ... $_{PDR}$.

opaque. In order to determine whether the drawing process results in a pure uniaxial deformation, the width and thickness of the tapes were measured and compared to the theoretical values obtained for a laterally homogeneous deformation at constant volume. It can be seen from Figure 5 that the measured values match the theoretical prediction. This implies that the tapes were uniaxially deformed while drawing and the post-draw ratio λ_{PDR} is uniquely determined by the ratio of winder speed to godet speed. However, a slight deviation of the measured width from the theoretical predictions is noticeable for $\lambda_{PDR} > 10$. Assuming a constant volume and a homogeneous deformation in the lateral dimensions, it follows that

$$\lambda_{PDR}\, wt = w_0 t_0 = const. \qquad (3)$$

The observed increase in normalized width seen in Figure 5(a) as compared to the predicted values means that the constant volume assumption is violated. This deviation is coherent with a change of the

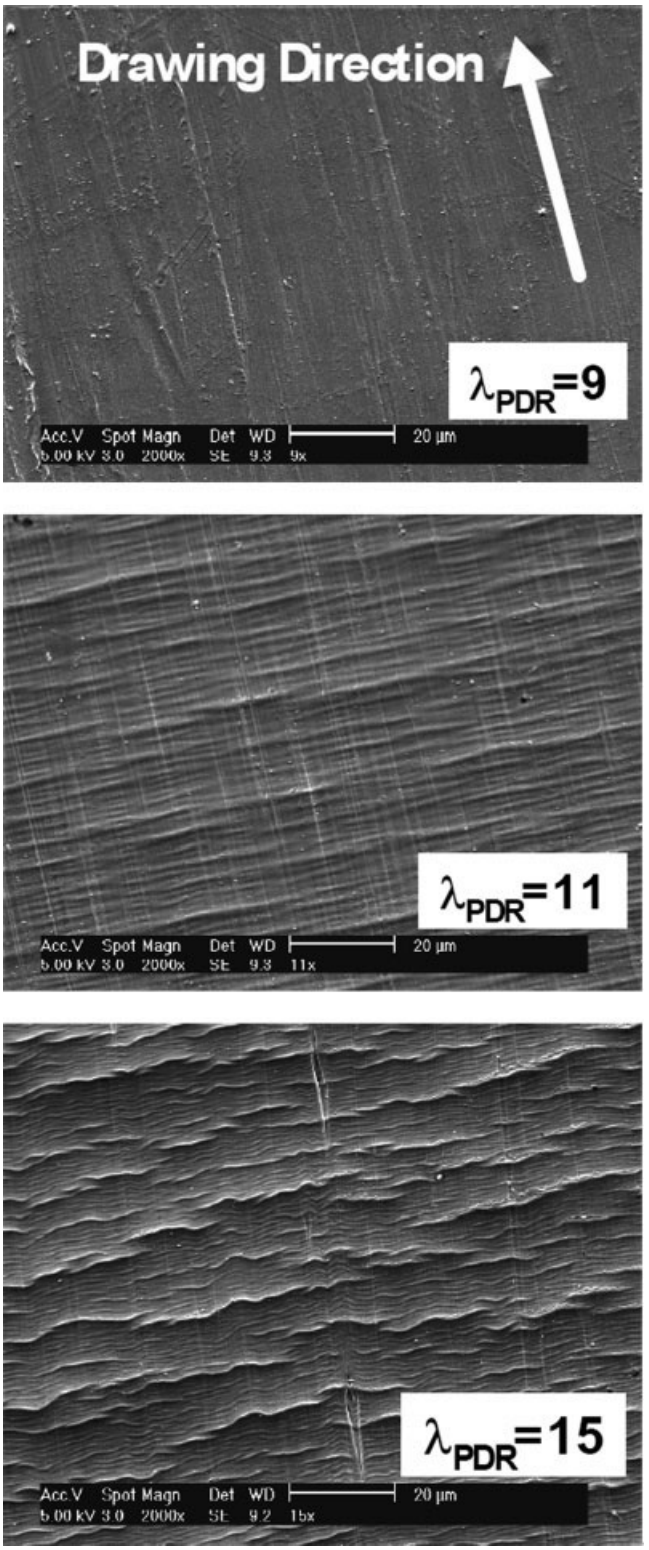

Figure 6 LVSEM images of the surfaces of the drawn tapes with $\lambda_{PDR} = 9$, $\lambda_{PDR} = 11$ and $\lambda_{PDR} = 15$, respectively.

optical appearance of the tapes (Fig. 4). Tapes post-drawn to $\lambda_{PDR} < 10$ are transparent over the whole sample width. A hardly visible opaque layer starts to develop in the centre of the tape with $\lambda_{PDR} = 10.5$. This layer widens with a further increasing post-draw ratio, resulting in a completely opaque tape at $\lambda_{PDR} = 11$.

The surface morphology of the post-drawn tapes with $\lambda_{PDR} = 9$, $\lambda_{PDR} = 11$, and $\lambda_{PDR} = 15$, respectively, were investigated by LVSEM (Fig. 6). The tape with $\lambda_{PDR} = 9$ possesses a smooth surface. The surface of the tape with $\lambda_{PDR} = 11$ shows a slightly developed pattern perpendicular to the drawing direction. At a post-draw ratio of $\lambda_{PDR} = 15$, the surface pattern becomes clearly developed with an arrangement of transverse bands separated by wormlike structures. After permanganic etching of the tape with $\lambda_{PDR} = 15$, a regular alignment of holes parallel to the drawing direction is observable within the transverse bands, as shown in Figure 7 at a higher magnification.

Additional confocal laser scanning microscopy investigations were performed on the tape with $\lambda_{PDR} = 15$ to further prove if the observed morphological feature is limited to the surface or extends into the bulk of the tape. The results are shown in Figure 8. From the cross-section images, one can observe that the surface morphology extends into the bulk of the tape. The decreasing intensity of the signal with increasing penetration depth results from the large scattering in the tape. However, the propagation of the surface morphology is recognizable up to a depth of about 20 μm. The onset of overdrawing is also reflected in density measurements (Fig. 9). The average density drops from about 902 kg mol^{-1} at $\lambda_{PDR} \leq 10$ to about 894 kg mol^{-1} at $\lambda_{PDR} > 10$. The densities of the tapes with $\lambda_{PDR} = 14$ and $\lambda_{PDR} = 15$ were even below the range of the density column. The slightly higher densities of the tapes with $\lambda_{PDR} = 2$, 3, and 4 might result from an inhomogeneous post-drawing process. The tapes exhibit small regions, especially at post-draw ratios of 2 and 3, which are visible to the naked eye and are not regularly drawn.

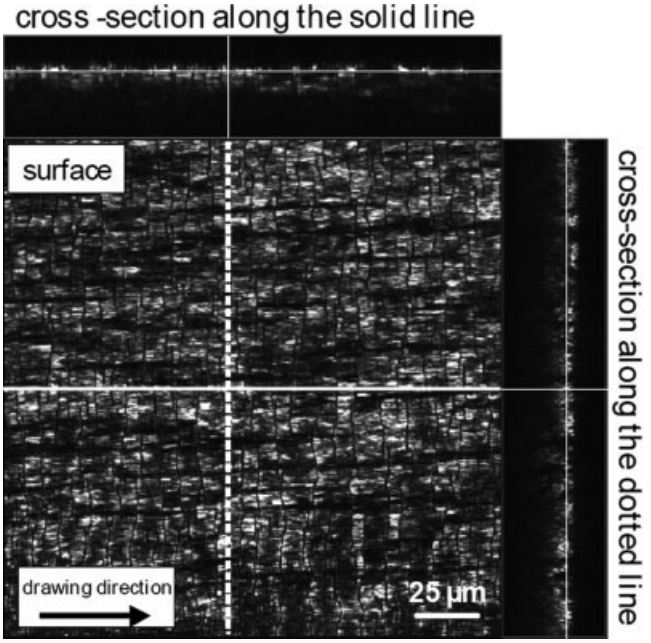

Figure 8 Confocal laser scanning microscopy images of the surface and of cross-sections (at the top: along the tape direction; on the right: perpendicular to the tape direction) of the tape with $\lambda_{PDR} = 15$.

As shown in Figure 10, the wide-angle X-ray patterns (each of the patterns was individually optimized in contrast and brightness) of the tapes clearly display the development of a fiber pattern with increasing post-draw ratio. The improved alignment of the crystals with respect to the drawing direction is revealed by the decreasing arc-length of the reflections with increasing draw ratio. It is noticeable that the pattern of the tape with $\lambda_{PDR} = 4$ also exhibits (110)-reflections in the meridional direction. These

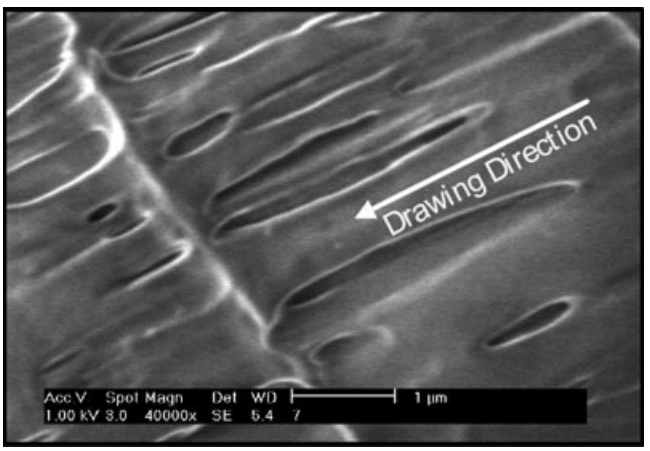

Figure 7 LVSEM image of the surface of the post-drawn tape with $\lambda_{PDR} = 15$ after permanganic etching.

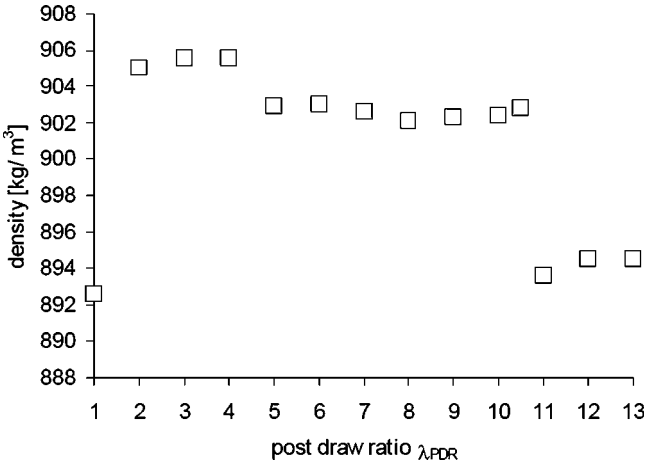

Figure 9 Plot of the average density of the tapes versus post-draw ratio.

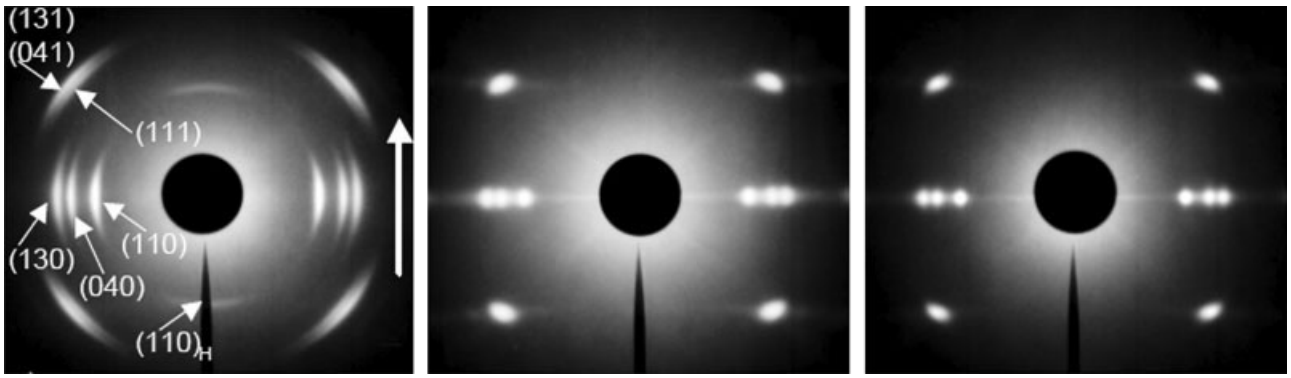

Figure 10 Wide-angle X-ray diffraction patterns of the drawn tapes with $\lambda_{PDR} = 4$ (left), $\lambda_{PDR} = 9$ (centre), and $\lambda_{PDR} = 15$ (right). The drawing direction is indicated by the arrow.

reflections indicate a homoepitaxial crystal growth of secondary lamellae onto primary lamellae (cross-hatching). In Figure 10 the reflections are indicated by the suffix 'H'.

In Figure 11(a), the FWHM values of the azimuthal intensity distribution, as the normalized measure of the arc length, are shown as a function of the post-draw ratio. For low post-draw ratios, the FWHM-values decrease rapidly with increasing draw ratio. At a draw ratio of about $\lambda_{PDR} = 6$, a plateau value is reached, and no relevant change in the FWHM values can be observed with further increase in draw ratio. However, to increase the sensitivity of small deviations in the plateau region, the reciprocal FWHM values were calculated [see Fig. 11(b)], and a significant drop is seen for $\lambda_{PDR} > 10$.

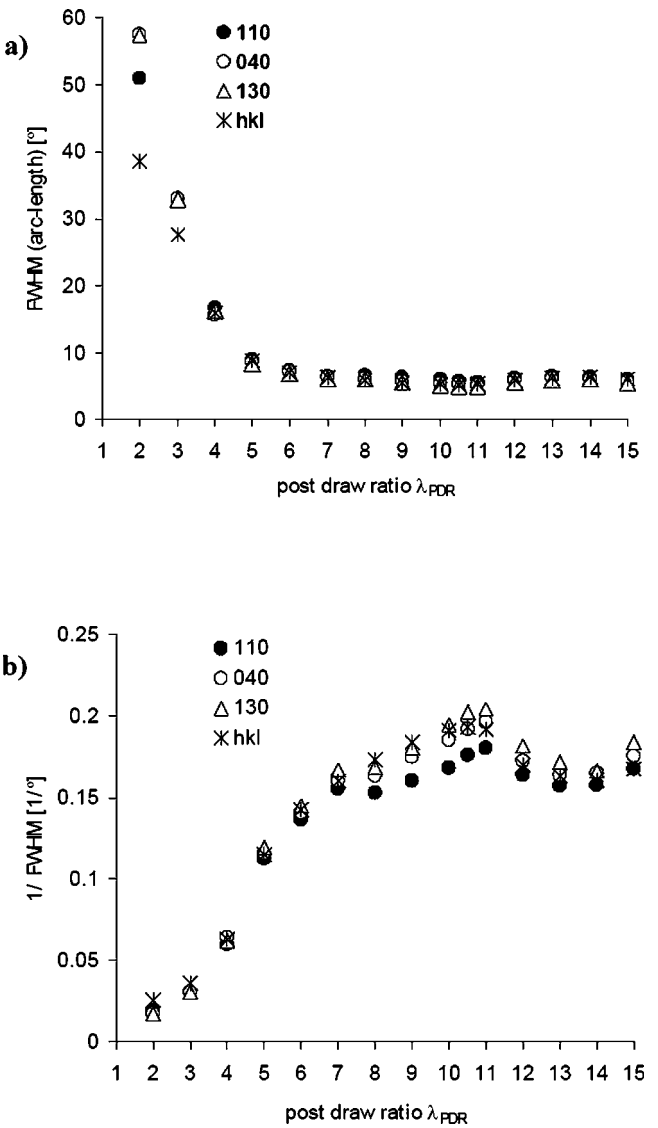

Figure 11 (a) FWHM and (b) 1/FWHM as a function of the post-draw ratio; 'hkl' represents the (111), (041), and (131) reflections, respectively, which are blurred at higher draw ratios.

Influence of the draw ratio on the mechanical properties

In Figure 12 sets of 10 individual stress–strain plots are shown for each of the post-drawn tapes. In Figure 12(a) the stress–strain plots of the tapes with $\lambda_{PDR} = 9$ to $\lambda_{PDR} = 14$, which are placed in-between the plots of tapes with $\lambda_{PDR} = 8$ and $\lambda_{PDR} = 15$, are left out in order to increase clarity. In Figure 12(b) the plots of the tapes with a relatively large elongation at break, $\lambda_{PDR} \leq 8$, are left out in order to spread the remaining stress–strain plots for $\lambda_{PDR} = 9$ to $\lambda_{PDR} = 11$, $\lambda_{PDR} = 13$, and $\lambda_{PDR} = 15$. The plots of the tapes with $\lambda_{PDR} = 10$, $\lambda_{PDR} = 10.5$, $\lambda_{PDR} = 12$, and $\lambda_{PDR} = 14$ are removed for clarity. From Figure 12, one can observe that the Young's modulus continuously increases with increasing post-draw ratio while the elongation at break decreases. The average values of the Young's modulus and the elongation at break are displayed in Figures 13(a) and 13(b), respectively. The average Young's modulus was graphically defined by measuring the gradient of the line which most closely fits

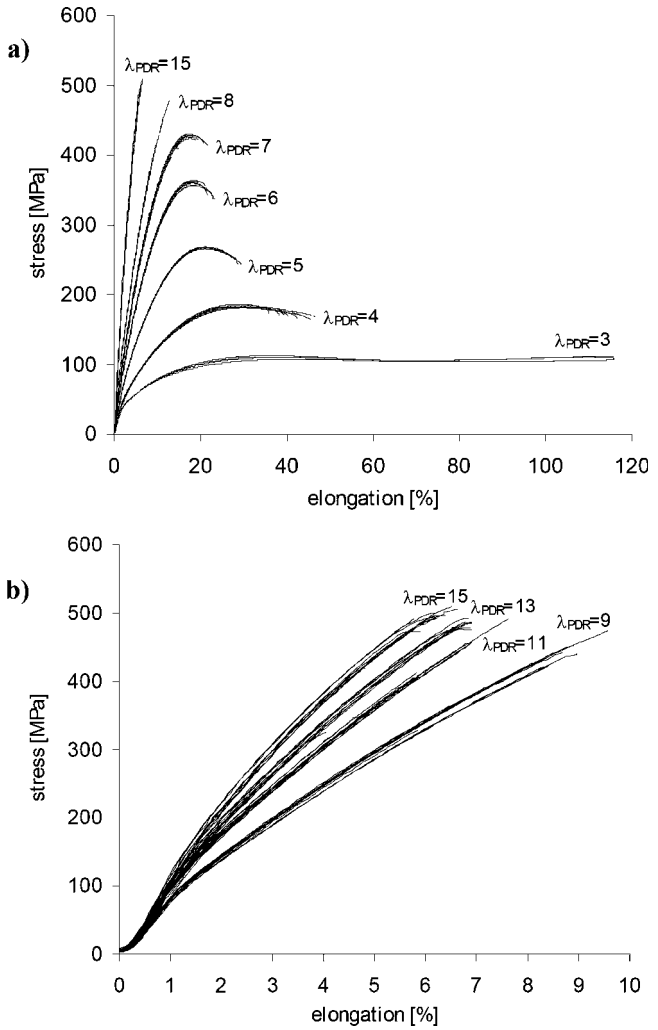

Figure 12 Stress–strain curves of the drawn tapes with (a) $\lambda_{PDR} \in (3, 4, 5, 6, 7, 8, 15)$ and (b) $\lambda_{PDR} \in (9, 11, 13, 15)$.

all individual stress–strain plots in the interval from 0.2 to 1% strain. The average elongation at break was calculated as the numerical average of the 10 individual measurements. It can be seen from Figure 13(b) that the standard deviation from the average value is small. At some post-draw ratios, all the individual values are hidden behind the open square of the average value. From Figure 12, one can also observe that the strength seems to reach a maximum value at approximately 500 MPa, since there is only a small increase observable from about 480 MPa for the tape drawn to $\lambda_{PDR} = 8$ to 510 MPa for the tape with $\lambda_{PDR} = 15$. Nevertheless, a systematic inspection of the tensile test results shows a peculiarity of the dependence of the strength on the applied post-draw ratio. In Figure 14 the strength of each individual tensile test experiment is represented by a small double cross. The open squares illustrate the average strength for each post-draw ratio. The average strength increases for $3 \leq \lambda_{PDR} \leq 7$, before leveling off at about 400 MPa for tapes with $7 \leq \lambda_{PDR} \leq 9$. At a post-draw ratio of $\lambda_{PDR} = 10.5$, the average strength decreases to about 350 MPa. Finally, the strength increases again to about 500 MPa for the completely overdrawn tape. At low post-draw ratios, $\lambda_{PDR} \leq 7$, the distribution of the individual strength values is quite narrow. In the drawing regime, where the transition from transparent to opaque appearance takes place, $9 \leq \lambda_{PDR} \leq 11$, the values spread out from about 220 MPa to about 480 MPa. Finally, the distribution becomes very small for tapes which are completely overdrawn ($\lambda_{PDR} \leq 13$).

The different value distribution of the individual strength measurements also has consequences with regard to the average energy absorption (work-to-break) of the drawn tapes. In Figure 15, the energy absorption, approximated by the area under the stress–strain plot, is shown as a function of the applied post-draw ratio in the solid-state drawing process. Three different levels of energy absorption can be distinguished. The tape with $\lambda_{PDR} = 3$ posses an

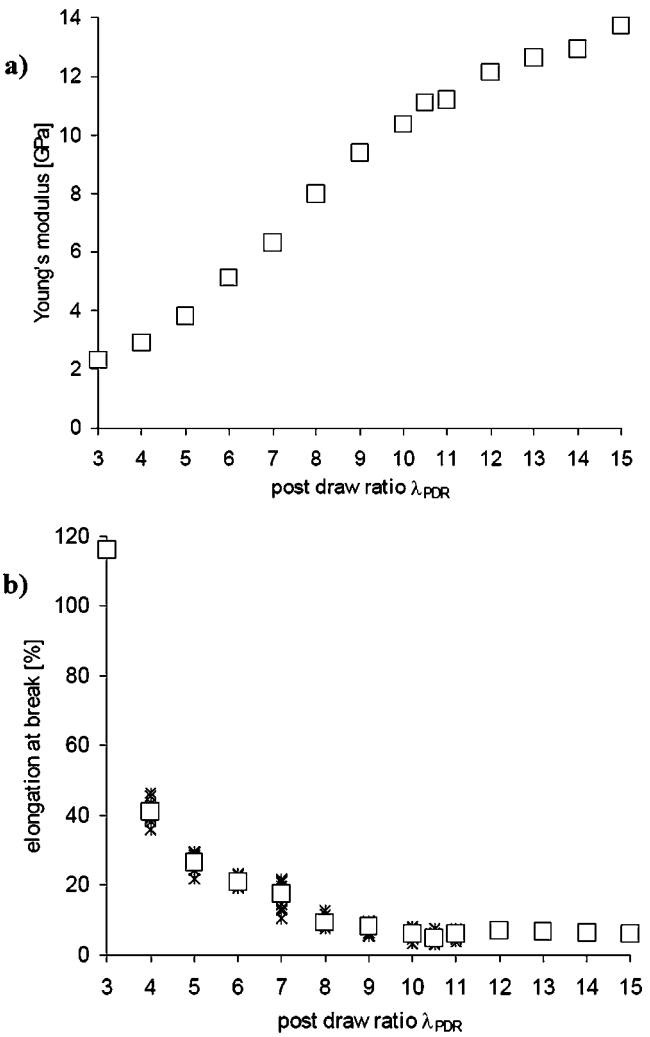

Figure 13 (a) Young's modulus and (b) elongation at break in dependence to the applied post-draw ratio. Open squares: the average values; small double crosses: the individual measurements.

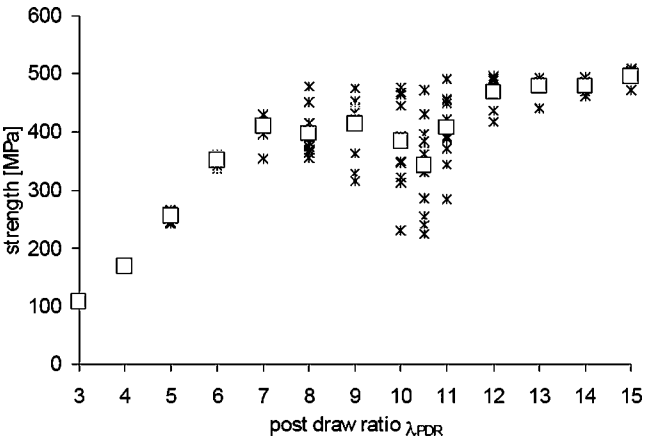

Figure 14 Strength as a function of post-draw ratio. Open squares: the numerical-average values; small double crosses: the individual measurements.

average energy absorption of about 11,600 arbitrary units. From its stress–strain plot in Figure 12(a), it follows that the high level of energy absorption results from deformation via neck formation on a relatively low stress level of about 100 MPa. The second distinct level of energy absorption is the plateau at about 5300 arbitrary units for the tapes with $\lambda_{PDR} = 4$ to $\lambda_{PDR} = 7$. All these tapes exhibit a yield point in their stress–strain plots. The decrease in the strain at break with increasing draw ratio is compensated by an adequate increase in the yield stress. The third level of energy absorption at about 1900 arbitrary units can be attributed to the tapes with $\lambda_{PDR} \in \{8, 9, 12, 13, 14, 15\}$. The decrease in energy absorption of about 3400 arbitrary units compared to the tape with $\lambda_{PDR} = 7$ can be explained by the disappearance of yielding. The large distribution in the individual strength measurements in the drawing regime, where the transition from transparent to opaque appearance takes place, is also accompanied by a large variation of the individual energy absorption. As a result, the average energy absorption drops by approximately 50% to about 960 arbitrary units for the tape with $\lambda_{PDR} = 10.5$. However, it should be noted that the completely overdrawn tape with $\lambda_{PDR} = 15$ can provide the same average energy absorption as the transparent tape with $\lambda_{PDR} = 8$, although its Young's modulus is approximately 70% higher (13.7 GPa for $\lambda_{PDR} = 15$ compared to 8 GPa $\lambda_{PDR} = 8$).

The abrasion resistance of the tapes with $\lambda_{PDR} = 7$ to $\lambda_{PDR} = 15$ is shown in Figure 16. For the tapes with $\lambda_{PDR} = 7$ and $\lambda_{PDR} = 8$, three individual measurements were performed. The tapes with $\lambda_{PDR} > 8$ were tested five times. The small double crosses display the results of the individual measurements; the large square represents the average value. In order to obtain normalized results, the number of cycles was divided by the cross-section area of the tape. The abrasion resistance per unit cross-section area decreases steeply with increasing draw ratio, followed by a gradual decrease at high draw ratios. However, the normalized abrasion resistance of about 2000 cycles $\cdot$ mm^{-2} for the transparent tape with $\lambda_{PDR} = 10$ halves to about 1000 cycles $\cdot$ mm^{-2} for the completely overdrawn tape with $\lambda_{PDR} = 15$.

The results of the shrinkage experiments are shown in Figure 17. Shrinkage decreases steeply from about 9% for the tapes drawn to $\lambda_{PDR} = 2$ and $\lambda_{PDR} = 3$ to about 5% for the tape with $5 \leq \lambda_{PDR} \leq 10$. Finally, the shrinkage decreases gradually to about 2.5% for the completely overdrawn tape with $\lambda_{PDR} = 15$.

DISCUSSION

In the results section above, we have shown that overdrawing of iPP tapes within the solid-state drawing process results in whitening of the sample. At a certain post-draw ratio, an opaque layer starts to de-

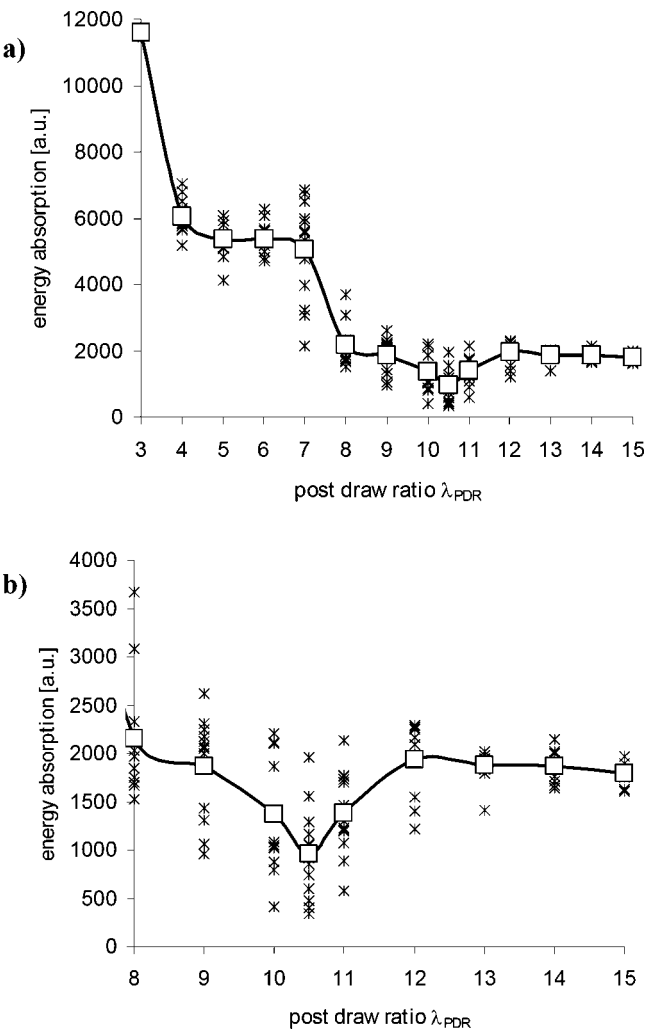

Figure 15 (a) Energy absorption as a function of the post-draw ratio; (b) details for $\lambda_{PDR} = 8$ to $\lambda_{PDR} = 15$. Open squares: the numerical average energy absorption; small double crosses: the individual measurements.

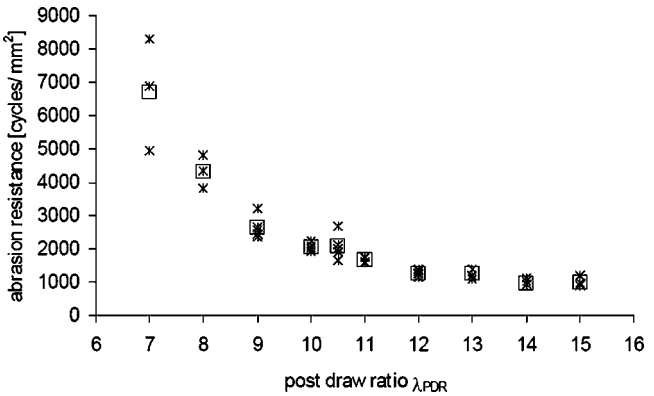

Figure 16 Abrasion resistance versus post-draw ratio, λ_{PDR}. Small double crosses: the individual measurements; open squares: the average values for each draw ratio.

velop in the centre of the former transparent tape. With increasing post-draw ratio, the opaque layer spreads over the complete tape width. The LVSEM (see Fig. 6) and CSLM (see Fig. 8) images show that the whitening is accompanied by morphological changes on the sample surface as well as in the bulk. Transparent tapes with $\lambda_{PDR} < 10$ possess a smooth surface. The surface of the tape with $\lambda_{PDR} = 11$ shows a slightly developed pattern perpendicular to the drawing direction. At a post-draw ratio of $\lambda_{PDR} = 15$, the surface pattern becomes clearly developed with an arrangement of transverse regions separated by wormlike structures. This surface structure was observed also by the Bassett group studying overdrawn iPP fibres.[16] They suggested that the formation of a regular arrangement of the transverse bands and the wormlike structures results from a deformation process where the sample is alternately drawn at two different draw ratios. Figure 18 shows the schematic force-elongation curve of the solid-state drawing process of overdrawn tapes. Generally, three kinetic modes of deformation processes can be distinguished[9] as follows.

i. In a conventional tensile test experiment, the tape is drawn with a constant extension rate (CER):

$$\varepsilon^{\bullet} = \left(t + \frac{l_0}{v}\right)^{-1} \tag{4}$$

where $\varepsilon^{\bullet}$ is the strain rate and v is the cross-head speed.

ii. Constant-strain-rate (CSR) drawing can be used to simplify the analysis of time-dependent effects. Usually, CSR drawing is also performed with tensile testing equipment, with the rate of extension being continuously increased to maintain constant rate of strain:

$$\lambda = \exp(\varepsilon^{\bullet} t) \tag{5}$$

iii. In a continuous fiber/tape drawing process, a constant force (CF) is applied on the tape while drawing:

$$F = const. \tag{6}$$

The described tape-preparation route corresponds to a CF drawing process, i.e., a constant force is applied on the tape in the drawing stage. If the applied post-draw ratio λ_{PDR}, as determined by the ratio of the winder speed to the godet speed, is located in-between λ_1 and λ_2, it is necessary to apply the constant force F_0 on the tape; otherwise, the tape cannot overcome the post-draw ratio λ_1. Consequently, a certain sequence of the tape is drawn directly to the ratio λ_2, which also corresponds to the applied force F_0. Therefore, this segment of the tape is drawn to a higher extent than adjusted by the ratio of the godet speed to the winder speed. This additional stretching can be compensated if the following tape segment is drawn to the ratio λ_1. The lengths of the segments are determined by the following relationships:

$$l_{01} + l_{02} = l_0 \tag{7}$$

$$l_{01}\lambda_1 + l_{02}\lambda_2 = l = l_0\lambda_{PDR} \tag{8}$$

where l_{01} is the initial length of the segment, which is drawn to λ_1; accordingly, l_{02} is the initial length of the segment, which is drawn to λ_2. The second equation ensures that the sum of the initial segments l_0 is drawn on average to the applied post-draw ratio λ_{PDR}.

It is worth mentioning that the force-elongation curve, shown in Figure 17, is different from a stress–strain plot obtained by a tensile test. The force-elongation curve is an individual curve for each draw ratio, i.e., the positions of λ_1 and λ_2 depend on the applied post-draw ratio λ_{PDR}. As indicated in Figure 18, the lower draw ratio λ_1 is related to the wormlike struc-

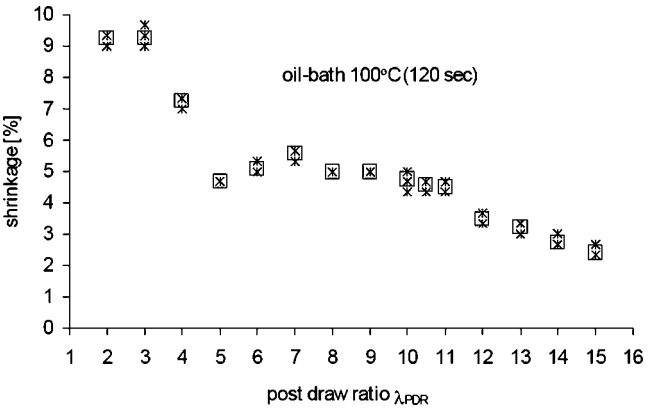

Figure 17 Shrinkage as a function of the post-draw ratio of the tape. Small double crosses: the individual measurements; open squares: the average values.

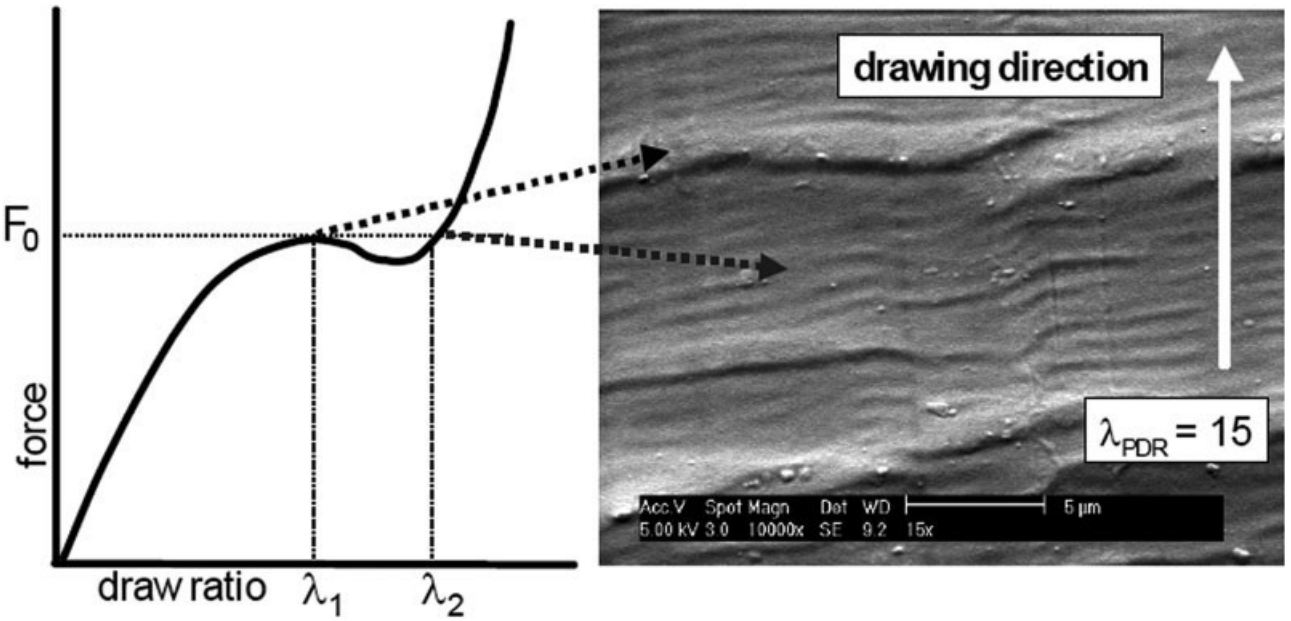

Figure 18 Schematic force-elongation curve of the manufacturing process of overdrawn tapes according to Abo El-Maaty et al.[16]

tures, while the higher draw ratio λ_2 can be related to the transverse regions in-between the worms. The LVSEM image of the permanganic etched tape ($\lambda_{PDR} = 15$) exhibits a regular alignment of holes parallel to the drawing direction within the transverse regions. The holes may be already present in the tape before etching or they may be imposed by the etching procedure. In the latter case, the holes are generated in regions where the density is much lower compared to the surrounding material, because the reduced density favors etching in these regions. It can be concluded that the transverse regions are fibrillated into regions of high density and low density, respectively. This statement includes the possible presence of holes before etching as the extreme of low density. As a result of the fibrillated structure in the transversal regions, the average density of the tape drops, as shown in Figure 9.

The fibrillated structure also explains the peculiarity in the development of the reciprocal FWHM values in the overdrawing regime, as shown in Figure 11(b). With respect to the drawing direction, a slight misalignment of individual fibrils, and the additional air-scattering (more precisely, 'low density-scattering') result in a more diffuse scattering pattern. It can be concluded that a completely overdrawn tape possesses a fibrillated structure, in which high-density regions are parallel aligned to the drawing direction and separated by low-density regions. A schematic drawing of this structure is shown in Figure 19(a). The differences in the homogeneity of the failure behavior can be explained by the morphology of the tapes. Completely overdrawn tapes possess a fibrillated structure over the whole width, which can be considered as a bundle of fibers or fibrils. A crack initiated in a fibril (high-density) meets with a low-density region (or hole). For further crack propagation, the crack has to be initiated again in the neighboring fibril, i.e., the low-density regions (or holes) can be considered to resist crack propagation. Therefore, the failure of individual fibril is accompanied only by a small loss of cross-section area of the tape. The remaining fibrils can easily resist the slightly increased stress. Consequently, the tape is not sensitive to a local failure of individual high-density fibrils. Instead, the strength of the tape more accurately reflects the average strength of all the fibrils. This results in an excellent regularity of the tensile behavior of the overdrawn tapes.

Accordingly, a tape drawn to a ratio where the opaque layer starts to develop in its centre has a morphology that is shown schematically in Figure 19(b). Here, the tape possesses density fluctuations in its centre and a bulky, transparent layer of constant density on its edges. The start of overdrawing in the centre of the tape can be explained by the higher axiality of the local stress in the center, resulting in a slightly biaxial deformation (in contrast to the pure uniaxial deformation at the edges of the tape). Due to the reduced number of fibrils compared with completely overdrawn tapes, the fibrillated structure in partially overdrawn tapes is more sensitive to a failure of individual fibrils. The loss of an individual fibril can result in a stress concentration in the remaining fibrils, leading directly to the failure of the whole fibrillated structure and, finally, to failure of the tape. Furthermore, the failure of the tapes might also arise from crack initiation in the transparent

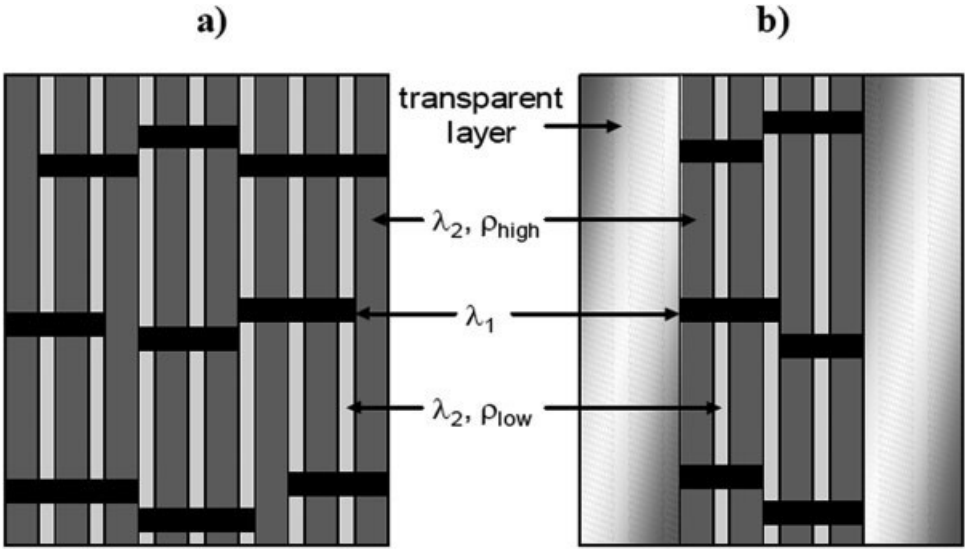

Figure 19 Schematic drawing of the morphology of drawn tapes: (a) completely overdrawn tape; (b) incompletely overdrawn tape where the opaque layer starts to develop in the centre. Black regions belong to wormlike features with λ_1; dark-gray and light-gray regions indicate high density with λ_2 and low density in the transversal band, respectively.

layers. Due to the absence of crack arresters such as the low-density regions in completely overdrawn tapes, a crack can propagate unhindered in these layers, resulting in a decrease of the supplying cross-section area and, finally, in the failure of the tape. It can be concluded that partially overdrawn tapes are highly sensitive to a local failure in their structure, thus explaining the large spread in strength of these tapes. The regularity of the tensile behavior of completely transparent tapes, on the one hand, may result from their homogeneous structure. On the other hand, it has to be considered that the tapes possessing the narrowest distribution in the values of strength ($3 \leq \lambda_{PDR} \leq 6$) exhibit yielding in their stress–strain curves, i.e., a relatively small stress window corresponds to a large range of elongation. Consequently, the tapes might have a narrow spread in their individual strength values, although they posses a large distribution in the individual elongation at break, as can be seen for the tape with $\lambda_{PDR} = 4$ in Figures 13(b) and 14.

From the presented tensile test data, it can be concluded that overdrawing benefits some mechanical properties. Within a series of tapes drawn to various draw ratios, the most overdrawn tape possesses:

i. an excellent uniformity in tensile behavior;
ii. the highest average strength and the lowest elongation at break;
iii. an excellent ratio of stiffness to energy absorption.

Moreover, the highest overdrawn tape possesses the highest tensile modulus and the lowest thermally induced shrinkage, which is a consequence of the ultimate applied draw ratio. The shrinkage behavior of the tapes depends on two effects acting against each other. Below the melting temperature, the shrinkage results primary from the relaxation of the amorphous phase. The entropy is the driving force for the shrinkage, i.e., the tendency to shrinkage increases with increasing chain orientation in the amorphous phase. Consequently, shrinkage should increase with increasing post-draw ratio. However, this is only valid for a serial alignment of the crystalline and amorphous phases. If the crystalline phase forms a continuous ''brick-wall'' structure, it will hinder the overall shrinkage. The perfection of such a network increases with increasing draw ratio. In Figure 17, one can see that the percentage of shrink steeply decreases from about 9% for the tape with $\lambda_{PDR} = 3$ to about 5% for the tapes with $\lambda_{PDR} = 5$. This decrease can be associated with the formation of a crystal ''brick-wall'' structure. The gradual decrease at higher draw ratios can be related to a further perfection of this structure. It can be concluded that the thermal stability of the tapes increases with increasing post-draw ratio, which again is an advantage for many applications.

However, the abrasion tests have shown a drawback of overdrawn tapes. They possess a lower abrasion resistance compared to the transparent tapes, which are not overdrawn. The loss in abrasion resistance results from the higher alignment of the polymer chains with respect to the drawing direction, which is connected with a reduced cohesion of the chains in the lateral directions. Furthermore, the fibrillated structure of the tapes enlarges the actual striking surface. In the abrasion test, not only the tapes themselves rub on each other, but also the individual fibrils within the tapes. Consequently, overdrawing is not desirable for applications requiring a high abrasion resistance, such

as ropes. The drawback of reduced abrasion resistance might be overcome by coating the overdrawn tape with a copolymer layer (coextrusion), thus sealing the fibrillated homopolymer core.

Finally, it has to be mentioned that the morphological features of overdrawn tapes are independent of processing conditions or material characteristics such as the average weight molar mass; however, these parameters determine the post-draw ratio for the onset of overdrawing. Studies on different iPP homopolymer grades have shown that the onset of overdrawing shifts, for example, towards lower post-draw ratios with increasing average weight molar mass.[19,20]

CONCLUSIONS

We have characterized the structure, morphology, and properties of melt-spun and solid-state drawn isotactic polypropylene tapes. For post-draw ratios above 10, the so-called overdrawing regime exists, where the appearance of the tapes changes from transparent to opaque. At the same time, several morphological features as well as the overall mechanical behavior of the tapes have altering effects as follows:

- Overdrawing results in whitening of the iPP tape being accompanied by morphological changes on the surface and in the bulk of the tape.
- Completely overdrawn iPP tapes possess a regular arrangement of transverse regions crossed by wormlike structures.
- The structural features can be attributed to a deformation process where the sample is alternately drawn at two different draw ratios: $\lambda_{\text{wormlike structure}} < \lambda_{\text{transverse region}}$.
- Overdrawing of iPP tapes results in improvement of some mechanical properties. The highest tensile modulus, highest strength, and lowest elongation at break were obtained in the most highly drawn tape. Moreover, this tape exhibits the lowest shrinkage at elevated temperatures.
- Due to their fibrillated morphology, completely overdrawn tapes behave like a bundle of fibers resulting in a more homogenous mechanical behavior and an increase of the average strength and the average energy absorption, compared to tapes that are not completely overdrawn.
- A reduced abrasion resistance is a drawback of overdrawn tapes.

The authors are grateful to the R&D team from Lankhorst Indutech B.V., The Netherlands, for their assistance during the tape manufacturing. We would like to acknowledge Novem for financial support of the PURE Project, within which the current studies were performed. The authors also thank Frank van de Burgt and Marco Hendrix for their support for X-ray investigations. Special gratitude is extended to Cees Bastiaansen for his indefatigable readiness for discussion.

References

1. Sheehan, W. C.; Cole, T. B. J Appl Polym Sci 8, 1964, 2359–2388.
2. Hoshino, S.; Powers, J.; Legrand, D. G.; Kawai, H.; Stein, R. S. J Polym Sci 58, 1962, 185–204.
3. Compostella, V.; Coen, A.; Bertinotti, F. Angewandte Chemie, 74, 1962, 618–624.
4. Nadella, H. P.; Henson, H. M.; Spruiell, J. E.; White, J. L. J Appl Polym Sci 21, 1977, 3003–3022.
5. Spruiell, J. E.; White, J. L. Polymer Engg and Sci 15, 1975, 660–667.
6. Kitao, T.; Ohya, S.; Furukawa, J.; Yamashita, S. J Polym Sci Pt B: Polym Phys 11, 1973, 1091–1109.
7. Lu, F. M.; Spruiell, J. E. J Appl Polym Sci 34, 1987, 1521–1539.
8. Lu, F. M.; Spruiell, J. E. J Appl Polym Sci 34, 1987, 1541–1556.
9. Salem, D. R. In Structure formation in polymeric fibres; Salem, D. R., Ed.; Hansers Publishers: Munich, 2000.
10. Bodaghi, H.; Spruiell, J. E.; White, J. L. Int Polym Processing 3, 1988, 100–112.
11. Hahn, K.; Kerth, J.; Zolk, R.; Schwahn, D.; Springer, T.; Kugler, J. Macromolecules 21, 1988, 1541–1543.
12. Diacik, I.; Durcova, O.; Mitterpachova, M. Acta Polymerica 39, 1988, 391–396.
13. Gill, R. A.; Benjamin, C. Plastic and Rubbers Processing 5, 1980, 25.
14. Andreassen, E.; Myhre, O. J.; Hinrichsen, E. L.; Grostad, K. J Appl Polym Sci 52, 1994, 1505–1517.
15. Irvine, P. A.; Smith, P. Macromolecules 19, 1986, 240–242.
16. Abo El-Maaty, M. I.; Bassett, D. C.; Olley, R. H.; Dobb, M. G.; Tomka, J. G.; Wang, I. C. Polymer, 37, 1996, 213–218.
17. Tung, L. H.; Taylor, W. C. J Polym Sci 21, 1956, 144–147.
18. Olley, R. H.; Hodge, A. M.; Bassett, D. C. J Polym Sci Pt B: Polym Phys 17, 1979, 627–643.
19. Schimanski, T.; Peijs, T.; Lemstra, P. J.; Loos, J. Macromolecules 37, 2004, 1810–1815.
20. Loos, J.; Schimanski, T. Macromolecules 38, 2005, 10678–10685.